Nanoscale

Accepted Manuscript

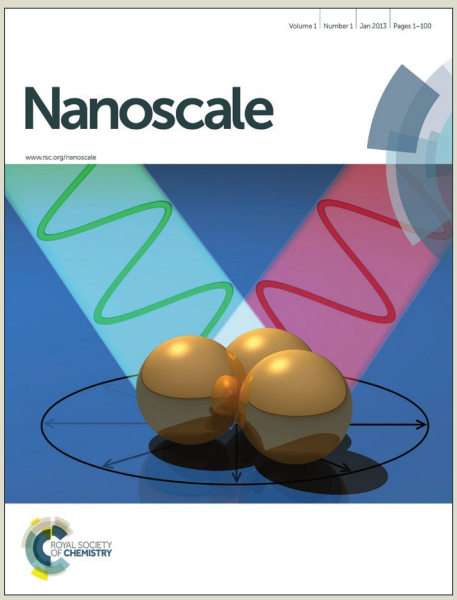

ROYAL SOCIETY OF CHEMISTRY

www.rsc.org/nanoscale

Nanoscale

PAPER

Manipulation of Combustion Waves in Carbon-Nanotube/Fuel Composites by Highly Reactive Mg Nanoparticles

Received 00th January 20xx,
Accepted 00th January 20xx

DOI: 10.1039/x0xx00000x

www.rsc.org/

Kang Yeol Lee, Hayoung Hwang, Dongjoon Shin, and Wonjoon Choi*

Manipulating the interface of micro/nanostructured materials and chemical fuels can change the fundamental characteristics of the combustion waves that are generated during a reaction. In this study, we report that Mg/MgO nanoparticles actively amplify the propagation of combustion waves at the interface of multi-walled carbon nanotubes (MWCNTs) and chemical fuels. Fuel/MWCNT and fuel/MWCNT-Mg/MgO composite films were prepared by a facile synthetic method. We present a complete physiochemical characterization of these composite films and evaluate the propagating velocities and real-time surface temperatures of the combustion waves. Mg/MgO nanoparticles at the interface enhanced reaction front velocity by 41%. The resulting explosive reactions supplied the additional thermal energy to the chemical fuel, accelerating flame propagation. Furthermore, the surface temperatures of the composites with Mg/MgO nanoparticles were much lower, seeing how the transient heat from the reaction would ignite unreacted fuels at lower surface temperatures despite not reaching the necessary activation energy for a chain reaction. This mechanism contributed to thermopower waves that amplified output voltage. Furthermore, large temperature gradients due to the presence of nanoparticles increased charge transport inside the nanostructured material, due to increased thermoelectric effects. This manipulation could contribute to the active control of interfacially driven combustion waves along nanostructured materials, yielding many potential applications.

Introduction

Combustion is one of the most widely applied methods for eliciting chemical, thermal, and electrical conversion. When combustion reactions are guided by specific conditions, such as confined geometries and contact with thermally conductive materials, the resulting combustion waves evolve in a highly anisotropic manner along the material interface. Within the last decade, micro- and nanotechnologies have been increasingly applied as a method of managing the produced combustion waves more effectively, as they allow for higher reactivity and improved control of the confined geometry. This suppression of isotropic energy release has been implemented in developing microthrusters,[1, 2] microactuators,[3] and microreactors,[4] as the limited space and narrow path for energy release significantly amplify specific impulse.[5, 6]

Meanwhile, other approaches have implemented highly reactive nanostructures. Many different nanothermites composed of metal/metal oxide nanoparticles have been studied to promote the initiation and reaction rate of combustion waves, with implementation in propellants, explosives, and pyrotechnics due to their need for high reactivity.[7-10] In addition, embedded, thermally conductive nanostructured materials in solid fuels have enabled the manipulation and guidance of combustion waves by means of interfacially-thermally driven chemical reactions by altering the interface.[11] Theoretical work has proven that the rate of combustion at the interface is highly dependent on the thermal properties of these embedded materials.[12, 13] Specifically, hybrid composites composed of carbon nanotubes (CNTs) and chemical fuels were able to generate these kinds of self-propagating waves.[14-17] The reaction rates of ZnO,[18, 19] MnO_2,[20] and Cu_2O-CuO[21] nanostructures have also been tested to confirm the reaction rates at the interfaces. However, all these approaches have used nanostructured materials as passive interfacial surfaces only. If active manipulation is possible in the identical nanostructured materials, it could help us to better understand and apply this interfacially driven combustion waves to technologies.

Herein, we introduce a new method for interfacial manipulation of combustion waves using highly reactive metal nanoparticles embedded in large area two-dimensional multi-walled CNTs (MWCNTs) thin films containing chemical fuels. Mg nanoparticles were used to accelerate the reaction rates in combustion waves as the active material because they ignite at 470 °C in air, providing the necessary added energy at a relatively low temperature compared with bulk materials.[22] Simple synthetic methods were used to produce both pure MWCNTs and the Mg/MgO functionalized MWCNTs, while the hybrid composites that have the interface between chemical fuel layers and prepared films were synthesized by wet

[a] School of Mechanical Engineering, Korea University (BK21+), Seoul, Korea, 136-701. E-mail: wojchoi@korea.ac.kr

[b] †Electronic Supplementary Information (ESI) available: Scheme of preparation of MWCNTs and MWCNT-Mg films; characterization of MWCNTs-$Mg(NO_3)_2$ composite; and distribution of Mg/MgO nanoparticles. See DOI: 10.1039/x0xx00000x

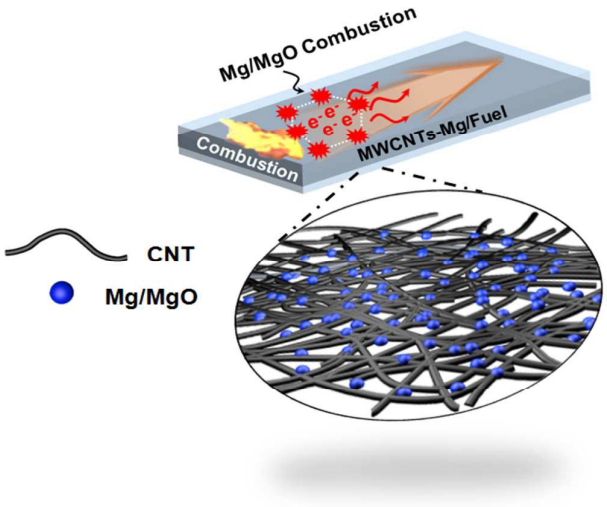

Fig. 1 Amplification of combustion and thermopower waves through the placement of Mg/MgO nanoparticles at the interface between chemical fuels and MWCNTs.

impregnation. A complete analysis of the composites confirmed good distribution of the nanoparticles on MWCNTs. The Mg/MgO nanoparticles provided the rapid, additional momentum energy with its low ignition temperature in combustion waves, and it resulted in the amplification of reaction rate, driven by interfacially amplified reaction rates, as shown in Figure 1. In addition, as an application of the amplified combustion wave, the output voltage generation of both thin film variants from thermopower waves was tested to assess whether their performance might merit future applications. Such voltage generation should be possible because combustion waves can induce charge carrier transport inside the nanomaterials, resulting in the concomitant generation of electrical energy, described in thermopower waves.

Experimental section

Chemicals

MWCNTs (diameter = 20-40 nm) were purchased from Jeio. *N,N*-dimethylformamide (DMF), diethyl ether, and magnesium nitrate hexahydrate ($Mg(NO_3)_2 \cdot 6H_2O$, 99%, 256.41 g/mol) were purchased from Aldrich. Collodion (5% nitrocellulose in 3/1 dimethylether/EtOH) was purchased from Kanto. All reagents were used as received without further purification.

Preparation of MWCNTs films

The MWCNTs were cleaned by sequential sonication in toluene, acetone, and diethyl ether. Next, 5.0 mL of deionized water was taken in a vial along with 4.0 mL of diethyl ether, yielding a biphasic mixture with the organic part on top and the aqueous section below. Then, 1.0 mL of a DMF solution of MWCNTs was added to this mixture, immediately forming a thin film at the interface.

Preparation of MWCNTs-$Mg(NO_3)_2$ composite films

The MWCNTs were cleaned in the same manner as described above. Then, 5.0 mL of aqueous $Mg(NO_3)_2$ (10 mM) was taken in a vial, to which was added 1.0 mL of MWCNTs solution in DMF. After sitting for 5 min, 5.0 mL of diethyl ether was added to this mixture, yielding a biphasic mixture with the organic part on top, the aqueous solution below, and a black thin film at the interface. This biphasic mixture was poured into a petri dish and the diethyl ether phase was evaporated, leaving a uniform thin film on the surface of the water. The film was then deposited on SiO_2/Si substrates without any additional purification (see Figure S1 and Figure S2).

Preparation of MWCNT-Mg/MgO composite film

The prepared MWCNTs-$Mg(NO_3)_2$ composite films, deposited on SiO_2/Si, were placed in the middle of a quartz tube in a horizontal tube furnace. They were then treated at 500 °C for 15 min under a reducing H_2 flow of 500 sccm. This yielded the target film on the SiO_2/Si substrate (see Figure S1).

Characterization of Materials

Scanning electron microscopy (SEM) images, energy-dispersive X-ray spectroscopy (EDX) mapping, and EDX line profile data were obtained using a field-emission SEM (FEI Model Quanta 250 FEG and Jeol Model JSM-6701F). Raman spectra were obtained using a Horiba Jobin Yvon LabRAM ARAMIS IR^2 spectrometer (532 nm diode laser as an excitation source). The Raman band of a silicon wafer at 520 cm^{-1} was used to calibrate the spectrometer. X-ray photoelectron spectroscopy (XPS) measurements were performed using an Ulvac-Phi X-tool spectrometer with an Al Kα X-ray (energy: 1486.6 eV) source. The base pressure of the chamber was about 1×10^{-10} Torr, while the electron takeoff angle was 90°.

Real-Time Measurements of Maximum Temperature and Reaction Velocity of Combustion Waves

The maximum temperature and reaction velocity of the combustion waves were evaluated by a setup designed for real-time measurement (Figure 1). A high-speed CCD camera (Phantom V7.3-8GB color camera) with a microscopic lens (Macro 105 mm, f/2.8D, Nikon) recorded the chemical reaction at a rate of 5000 frames/s. Combustion was initiated by tungsten Joule heating at the leading edge of the composites. Two optical pyrometers, a Raytek MM1MHCF1L and a Raytek MM2MLCF1L, were used to measure the temperatures of the films at the starting and ending positions of the chemical reactions, respectively. The first pyrometer measured the spectral response at the 1-μm position with a semiconductor photodetector with a temperature range of 560–3000 °C, whereas the second pyrometer measured the spectral response at the 1.6-μm position, with a semiconductor photodetector with a temperature range of 300–1100 °C.

Measurement of Output Voltage from Thermopower Waves

Copper electrodes were placed in contact with the composites at both ends. A Tektronix DPO2004B oscilloscope, set to an input impedance of 1 MΩ, was used to record the output voltage signal in real time.

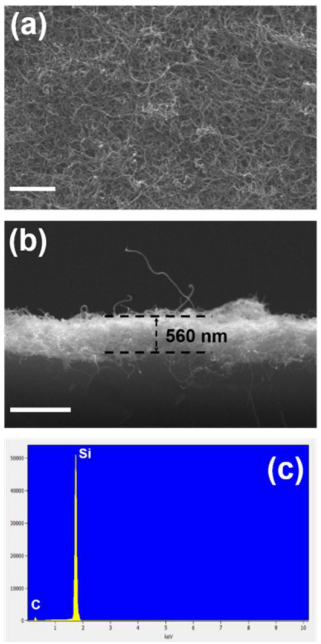

Fig. 2 (a) Top view and (b) cross-sectional SEM images of pristine MWCNTs film on a SiO2/Si substrate, along with the (c) EDX spectrum of said film. Scale bars are 1 μm.

Results and Discussion

MWCNTs thin film as interfacial layers for combustion waves was fabricated by a facile solution-phase method (Figure S1). MWCNTs in DMF solution was added to biphasic mixture of the diethyl ether (top layer) and DI water (bottom layer), and the mixed solution was gently homogenized. The MWCNTs which was immediately transferred to the aqueous phase, formed a thin film layer at the organic/water interface. Without further purification, transferring the MWCNTs layer to solid substrates allowed to collect the interfacial-thin film of MWCNTs. In details, the biphasic mixture was poured on a glass Petri-dish and the complete evaporation of the diethyl ether phase resulted in the formation of a uniformly thin film on the water surface. This MWCNTs film was deposited on SiO2/Si substrate, and it maintained stable contacts and structures for further development of the experimental platform.

The physicochemical properties of the pristine MWCNTs films were consistent with what was expected given the desired structure. Low and high magnification SEM showed the microstructures and morphology of the films, as shown in Figure 2a and 2b, respectively. The films uniformly covered the SiO2/Si substrate with a thickness of about 560 nm, with random orientation of the MWCNTs. The EDX spectrum clearly confirmed a composition of just C and Si (Figure 2c).

The reduction process was applied to fabricate MWCNTs-Mg composites, which was obtained from the transition of MWCNTs and MWCNTs-Mg$(NO_3)_2$ (see experimental section for details). As shown in Figure 3, Raman spectra confirmed the sequential formation of both MWCNT-Mg$(NO_3)_2$ and MWCNT-Mg, based on observed patterns consistent with previous research.[23] First, both the ratio between the D and G

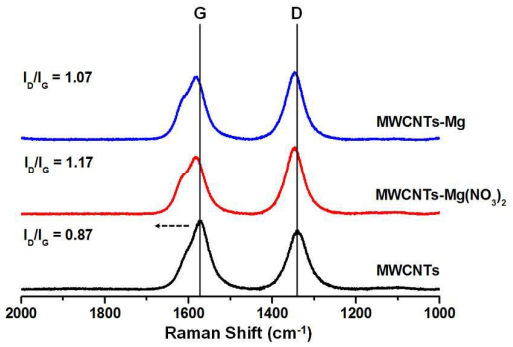

Fig. 3 Raman spectra of pristine MWCNTs film (black line), MWCNTs-Mg$(NO_3)_2$ film (red line), and MWCNTs-Mg film (blue line).

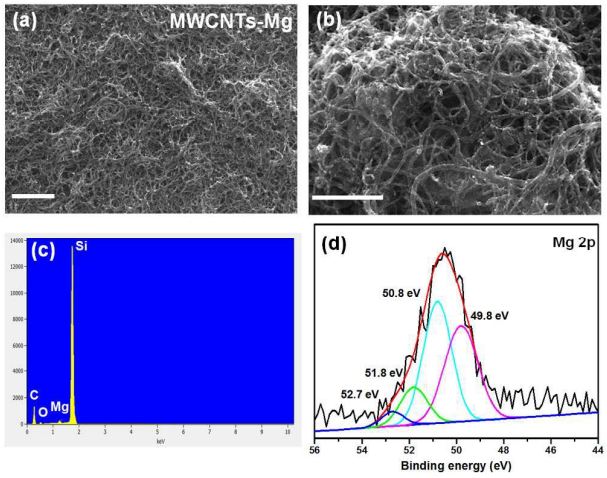

Fig. 4 (a) Top view SEM image, (b) magnified SEM image, (c) EDX spectra, and (d) XPS spectrum (black line) and Mg 2p peak deconvolution of MWCNTs-Mg. Scale bars are (a) 1 μm and (b) 500 nm.

bands (ID/IG) and the bandwidth of the G band for both MWCNTs-Mg$(NO_3)_2$ and MWCNTs-Mg were significantly greater than those of the pristine MWCNTs films. This transition indicates a clear increase in the number of defects of the CNT lattice.[24] Moreover, the composites showed a shift in the peak position of the G band, with MWCNTs-Mg$(NO_3)_2$ and MWCNTs-Mg moving upward by about 9.5 and 8.5 cm-1, respectively. This effect has been attributed to changes in the phonon structure, as well as the coupling of isoenergetic electronic states above the shifted Fermi level due to charge transfer between the CNTs and the functional groups.[25]

Figure 4a shows the SEM image of the MWCNTs-Mg film, with randomly-oriented networks of MWCNTs and embedded Mg nanoparticles visible throughout. Apparently, the general MWCNTs network structure was retained even after the reduction process was complete. Magnified images show selective embedding of round nanoparticles on the outer surfaces of MWCNTs (Figure 4b). The composition of the nanoparticles was determined by EDX (Figure 4c), which clearly shows Mg peaks. Particle sizes ranged widely from 10 to 50 nm, with the majority being no more than 30 nm (Figure S3).

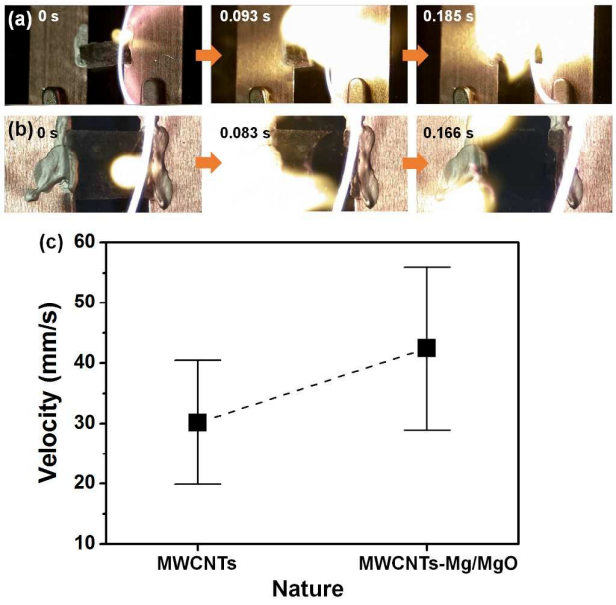

Fig. 5 Real-time snapshots of the propagation of combustion waves for (a) fuels/MWCNTs and (b) fuels/MWCNTs/Mg-MgO systems. (c) Comparison of average reaction velocities for the pictured reactions.

Because Mg nanoparticles are so reactive, it should be confirmed that the nanoparticles do in fact exhibit the expected composition. XPS can provide this highly detailed information, and has the added benefit of being nondestructive, with only those photoelectrons that escape the material without undergoing inelastic scattering being taken into account. To resolve the spectra of the MWCNTs-Mg composite, the energy scale was first calibrated with the C1s carbon contamination peak at 284.6 eV. The intrinsic binding states of the Mg 2p spectrum and the corresponding peaks deconvoluted as Gaussian components are shown in Figure 4d. Four binding energy peaks were observed at 49.8, 50.8, 51.8, and 52.7 eV, with the first two, the major peaks, clearly indicating the presence of metallic magnesium26 and MgO,27 respectively. Meanwhile, the last two minor peaks can be assigned to nonzero-valent states, corresponding to Mg(OH)228 and crystalline MgO/Mg(OH)x29 on the film surface, respectively. This XPS analysis reveals that the surface Mg cations were almost fully reduced by hydrogen gas at 500 °C, while the high reactivity of the resulting nanoparticles allowed for a quick reaction with oxygen. Furthermore, water molecules on the surface of the Mg nanoparticles were dissociated through an autocatalytic effect, yielding the small quantities of Mg(OH)2 and MgO/Mg(OH)x observed. Actually, MgO can be quickly formed by hydrogen gas.

$$Mg(NO_3)_2 + H_{2(g)} \rightarrow MgO + H_2O(g) + 2NO_{2(g)} \quad @\ 500\ °C$$

At the same time, MgO can be reduced by hydrogen gas in mixed complexes of MgO-CNTs at 500 °C,[30] and the MgH_2 is presented on the surface of Mg nanoparticles. In addition, CNT-Mg^{2+}-H_2 complexes interacted with the surfaces of CNTs can be reduced by electrons, provided from CNTs and H to Mg cation at relatively lower temperature than only Mg cases.31 According to this mechanism, the energy state of CNTs-Mg2+-H2 complexes is unstable more and more by increasing the surrounding temperature. As a result, the Mg hydride (MgH_2) on MWCNTs can be immediately deformed by hydrogen molecules from MgH_2 to Mg over 400 °C, and MWCNTs-Mg (Mg nanoparticles decorated on MWCNTs) can be obtained, as shown in the following stoichiometric reaction.[30]

$$MgO + H_2 \rightarrow Mg + H_2O \quad @\ 500\ °C$$

$$Mg + H_2 \rightarrow MgH_2$$

$$MgH_2 \rightarrow Mg + H_2 \quad @ > 400\ °C$$

Although this reduction process was implemented to MWCNTs-$Mg(NO_3)_2$, the part of that might be quickly oxidized as MgO, which was indicated in XPS data (Figure 4d), while the remained quantities of $Mg(OH)_2$ and $MgO/Mg(OH)_x$ were negligible. Therefore, it is concluded that the final composite film is composed of Mg, MgO nanoparticles and MWCNTs (MWCNTs-Mg/MgO).

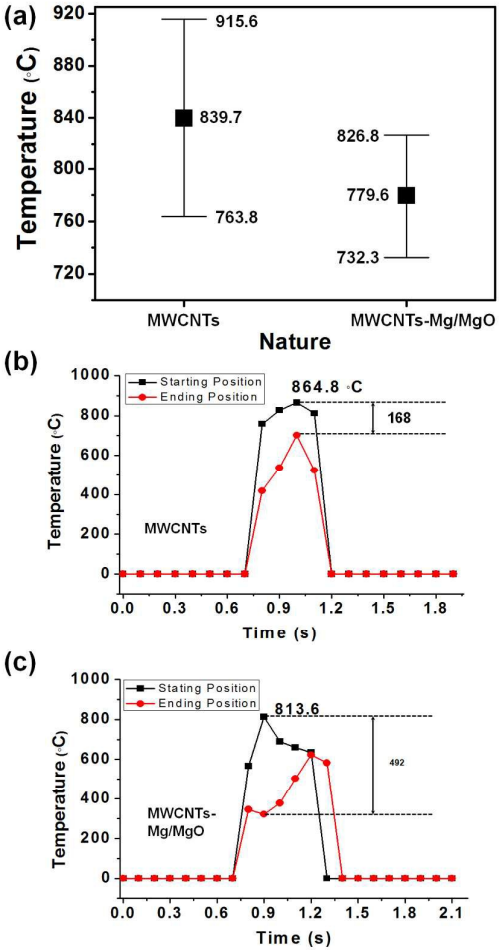

Fig. 6 (a) Surface temperature comparison of the fuels/MWCNTs and fuels/MWCNTs/Mg-MgO films. Surface temperature of the (b) fuels/MWCNTs and (c) fuels/MWCNTs/Mg-MgO composites, including the (1) starting and (2) ending positions of the combustion waves.

To investigate the specific effects of the addition of Mg nanoparticles for the propagation of combustion waves, the wet impregnation was applied to form the hybrid composites thin films of the chemical fuels and MWCNTs and MWCNTs-Mg/MgO, respectively, as described in the experimental section. The tungsten Joule-heating ignition at one end of the hybrid composites (0 s at Figure 5a) was used to launch the combustion waves at the interfaces of fuels/MWCNTs and fuels/MWCNTs-Mg/MgO hybrid composite films. Figure 5a and 5b shows the self-propagating combustion waves along the synthesized films, with the measurements beginning at the point of Joule heating ignition at one of the composites. The average reaction front velocity for the fuels/MWCNTs films was 30.15±10.26 mm/s, while that of the fuels/MWCNTs-Mg/MgO films was 42.41±13.49 mm/s (Figure 5c). The both average values were extracted from 31 testing devices. This 41% enhancement of reaction rates is due to the high reactivity of Mg nanoparticles, which is far greater than the normal reactivity of bulk Mg given the smaller particle sizes. For this reason, nanoparticles, especially those of Mg, typically only need a fraction of the activation energy that their bulk counterparts do, with necessary temperatures frequently dropping below 600 °C.[32] The self-propagating chain reaction was enough to supply the activation energy for Mg nanoparticles, and the high energy from explosive reaction of Mg/MgO nanoparticles could reaccelerate the combustion waves along the films.

The surface temperatures during the wave propagation can help to better understand the mechanism of wavefront propagation and the resulting velocity. The two optical pyrometers (a Raytek MM1MHCF1L and a Raytek MM2MLCF1L) were focused on the surfaces of hybrid composites films at the starting and the ending positions of the combustion waves, and they recorded the real time changes of surface temperatures of MWCNTs. While the combustion waves were propagated along the hybrid composites, each optical pyrometer tracked the temperature change at one fixed point on hybrid composites (either a starting position or a ending position of combustion). The high spatial and time resolutions of the optical pyrometers enabled the reliable temperature profile data in comparison with the total reaction time and hybrid composite size. In addition, since measurement interval of each optical pyrometer was longer than the required time that the combustion waves passed the focused area, it could track temperature change on specific positions. In the wave propagation, the major portion of required energy for rising temperatures is provided from chemical fuel layers, while the embedded Mg nanoparticles in composites amplify the reaction velocity of the combustion wave and promote the reaction of neighboring fuels. Figure 6a shows the average maximum surface temperatures during propagation, revealing a lower temperature for the fuels/MWCNTs-Mg/MgO film than for the fuels/MWCNTs film, with values of about average 779.6 and 839.7 °C among 10 testing devices, respectively. Apparently, the localized explosions over the Mg nanoparticles provided enough energy at those sites such that the required energy of the self-propagating reaction lowered overall. In case fuels/MWCNTs films, the only self-generating energy from the reacted chemical fuels had to overcome the activation energy to maintain the chain reaction to the neighboring-unreacted chemical fuels. However, in case fuels/MWCNTs-Mg/MgO films, the locally distributed nanostructured Mg particles provided the instant-high heat energy by discretized-explosive reactions to the neighboring-unreacted chemical fuels, and it resulted in lowering the required surface temperatures for the self-propagating chain reaction, like the 8 % (~ 60 °C) decrease in comparison with that of MWCNTs films.

Significant temperature differences between the starting and ending positions also reveal differences in the combustion waves, with values of 168 and 492 °C for the fuels/MWCNTs and fuels/MWCNTs-Mg/MgO films, respectively (Figure 6b and 6c). This tendency was also observed for other samples whose data are not presented. This follows from the described mechanisms; in the case of the fuels/MWCNTs samples, the reaction follows the interface, with thermal energy transferring all the way through to propagate the combustion waves, yet the nanoparticles in the fuels/MWCNTs-Mg/MgO samples could promote fuel consumption with less propagation of thermal energy. In details, for the fuels/MWCNTs film, the chain reaction of fuels is only following the interfaces of MWCNTs, and the released heat energy should be transported along the aligned direction of MWCNTs enough to maintain the combustion waves as the preheating zone for the chemical fuels. However, for the fuels/MWCNTs-Mg/MgO film, even though the released heat energy was not transferred enough to drive the chain reaction on the surface of MWCNTs, the highly energetic reaction of Mg/MgO nanoparticles could promote the combustion waves with relatively low preheating energy, and it resulted in the higher temperature differences between the starting and ending positions. It indicates that the introduction of Mg/MgO nanoparticles on the interface of MWCNTs would enhance the reactivity of the chemical fuels, since they are able to supply the explosive energy to overcome the activation energy barrier.

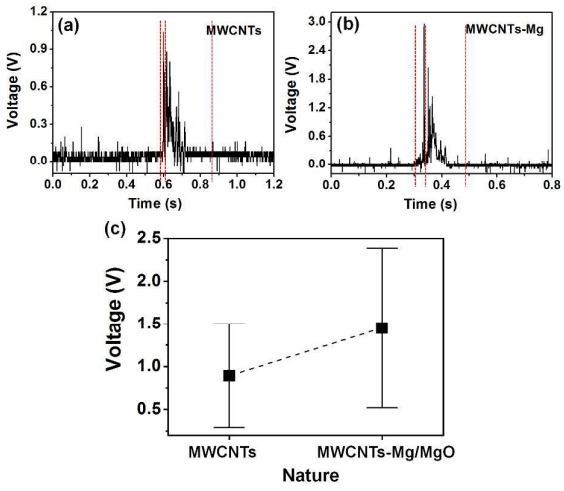

Fig. 7 Oscillatory voltage signal of the thermopower waves obtained from the (a) fuels/MWCNTs and (b) fuels/MWCNTs/Mg-MgO films. (c) Average output voltage of the two films.

As shown in Figure 5c (blue squares), the propagation velocities for the fuels/MWCNTs-Mg/MgO films were about 41% greater than those for the fuels/MWCNTs films. The introduction of Mg species may allow for the following four reactions to occur as part of combustion wave propagation.

$$MgO + C \rightarrow Mg + CO\uparrow \quad (1)$$

$$2Mg + O_2 \rightarrow 2MgO \quad (2)$$

$$MgO + H2O \rightarrow Mg(OH)_2 \quad (3)$$

$$Mg(OH)_2 \rightarrow MgO + H_2O\uparrow \quad (4)$$

Among all the listed Mg species, MgO is most likely to react with the MWCNTs. In general, any Mg nanoparticles on MWCNTs should be oxidized by air during the drying process. However, XPS analysis already demonstrated that this was not the case. In general, carbothermal reactions should occur as part of the combustion wave propagation; such reactions occur above 1400 °C on the macroscale,[33] yet only require activation temperatures of a bit over 900 °C when nanoscale MgO is present.[34] Moreover, the size difference of Mg particles from nanoscale to macroscale would highly vary the minimum-required temperature for ignition. For example, 200 nm Mg particles were ignited under 400 °C by the heat source.[35] The average diameter of Mg/MgO nanoparticles in the fuels/MWCNTs-Mg/MgO film was 19.3 nm, and it would be enough small to cause the specific size effect that lowered the required temperature around 800-1000 °C. Additionally, carbothermal reductions between amorphous bulk SiO_2 and bulk carbon typically occur above 1700 °C. However, in nanoscale reactions, controlled amounts of oxygen gas present due to chemical vapor deposition that generates one-dimensional nanotrenches on the SiO_2 layer at lower temperatures of about 900 °C; this dramatically lowers the required temperature to about 800 °C, allowing the reaction to occur. Also, the solid mixture of MgO and graphite significantly reduced the processing temperature. Therefore, lowering the required temperature would be feasible in the nanostructured composite of fuels/MWCNTs-Mg/MgO film.

When hybrid nanocomposites like these combust, thermal–chemical potential gradients on the surface are generated in the major nanostructures. Simultaneously, thermally excited charge carriers traveling in the propagating direction produce a concomitant electrical pulse, or a thermopower wave, that can be utilized by submicron- and nanosized power sources, as well as for the recovery of waste heat and residual fuels. Figure 7a and 7b show the typical output voltage signals from thermopower waves for both the fuels/MWCNTs and fuels/MWCNTs-Mg/MgO composites. The voltage profiles were divided into two distinct regions. The initial phase was during thermopower wave propagation, which lasted until the combusted fuel was consumed. During the initial phase, the moving temperature gradient resulted in a rise of output voltage. However, in the following decay phase, the voltage dropped back to zero as the system equilibrated to room temperature.

The fuels/MWCNTs-Mg/MgO composites showed an average output voltage of 1.450±0.933 V and a maximum output voltage of 4 V, significantly higher than the average output voltage of 0.892±0.603 V generated by the fuels/MWCNTs composite (Figure 7c). The both average values were extracted from 31 testing devices. Likewise, the addition of Mg nanoparticles improved the combustion wave velocity by 41%. This is consistent with the fact that accelerated combustion waves can amplify output voltage generation.[36] This value might also be affected by the real time temperature distributions shown in Figure 6b and 6c, as a larger temperature gradient can amplify charge transports due to increased thermoelectric effects. Furthermore, the low average temperatures in the fuels/MWCNTs-Mg/MgO films might correlate to the Thomson effect.[37] In this case, the charge carriers at one side of the electrode can travel to the other through the MWCNTs. This helps to reduce heat at the surface by means of taking the thermal energy from MWCNTs.

Conclusions

In summary, we demonstrated that the placement of Mg nanoparticles at the interface of MWCNTs and chemical fuels significantly enhanced combustion reaction rates. Both fuels/MWCNTs and fuels/MWCNTs-Mg/MgO films were prepared by a facile synthetic method. The discrete explosive reactions of Mg/MgO nanoparticles in the fuels/MWCNTs-Mg/MgO film amplified combustion wave velocities from 30.15 to 42.41 mm/s. The detailed mechanism of this new reaction was deduced through a complete analysis of the surface temperatures during combustion at both ends of the films. The average surface temperatures for the fuels/MWCNTs-Mg/MgO system was about 60 °C, or 8%, lower than that of the fuels/MWCNTs one, while the measured temperature gradient was much higher. This indicates that this discrete, highly energetic reaction supplies additional energy toward the activation of fuel combustion, despite the lower temperature and weak preheating conditions. The accelerated combustion waves and larger temperature gradient that resulted in turn contributed to more enhanced thermopower wave generation, with a 67% increase in output voltage; this was likely due in part to enhanced charge carrier transport along the MWCNTs. These results should help to improve the ability to actively control interfacially driven combustion waves along nanostructured materials. In addition, it provides a better understanding of the fundamental phenomena in chemical-thermal-electrical energy conversion, especially for micro/nanostructured materials, helping to extend upon current combustion, material synthesis, and energy conversion technology.

Acknowledgements

This work was supported by the Basic Science Research Program through the National Research Foundation of Korea (NRF), funded by the Ministry of Education, Science and Technology (NRF-2013R1A1A1010575), and by the Nano R&D program through the Korea Science and Engineering

Foundation, also funded by the Ministry of Education, Science and Technology (NRF-2012M3A7B4049863).

Notes and references

1 K. L. Zhang, S. K. Chou, S. S. Ang and X. S. Tang, *Sensor Actuat a-Phys*, 2005, **122**, 113-123.
2 C. K. Kuan, G. B. Chen and Y. C. Chao, *J Propul Power*, 2007, **23**, 1313-1320.
3 X. Zhou, M. Torabi, J. Lu, R. Q. Shen and K. L. Zhang, *Acs Appl Mater Inter*, 2014, **6**, 3058-3074.
4 W. C. Zhang, B. Q. Yin, R. Q. Shen, J. H. Ye, J. A. Thomas and Y. M. Chao, *Acs Appl Mater Inter*, 2013, **5**, 239-242.
5 K. D. Patel, M. S. Bartsch, M. H. McCrink, J. S. Olsen, B. P. Mosier and R. W. Crocker, *Sensor Actuat B-Chem*, 2008, **132**, 461-470.
6 A. Chaalane, C. Rossi and D. Esteve, *Sensor Actuat a-Phys*, 2007, **138**, 161-166.
7 C. S. Staley, K. E. Raymond, R. Thiruvengadathan, S. J. Apperson, K. Gangopadhyay, S. M. Swaszek, R. J. Taylor and S. Gangopadhyay, *J Propul Power*, 2015, **31**, 483-483.
8 H. Y. Wang, G. Q. Jian, G. C. Egan and M. R. Zachariah, *Combust Flame*, 2014, **161**, 2203-2208.
9 S. Apperson, R. V. Shende, S. Subramanian, D. Tappmeyer, S. Gangopadhyay, Z. Chen, K. Gangopadhyay, P. Redner, S. Nicholich and D. Kapoor, *Appl Phys Lett*, 2007, **91**.
10 C. S. Staley, K. E. Raymond, R. Thiruvengadathan, S. J. Apperson, K. Gangopadhyay, S. M. Swaszek, R. J. Taylor and S. Gangopadhyay, *J Propul Power*, 2013, **29**, 1400-1409.
11 V. V. Gubernov, V. N. Kurdyumov and A. V. Kolobov, *Combust Flame*, 2014, **161**, 2209-2214.
12 J. T. Abrahamson and M. S. Strano, *J Phys Chem Lett*, 2010, **1**, 3514-3519.
13 S. G. Mahajan, J. T. Abrahamson, S. Birkhimer, E. Friedman, Q. H. Wang, M. Beck and M. S. Strano, *Energ Environ Sci*, 2014, **7**, 3391-3402.
14 W. Choi, S. Hong, J. T. Abrahamson, J. H. Han, C. Song, N. Nair, S. Baik and M. S. Strano, *Nat Mater*, 2010, **9**, 423-429.
15 J. T. Abrahamson, B. Sempere, M. P. Walsh, J. M. Forman, F. Sen, S. Sen, S. G. Mahajan, G. L. C. Paulus, Q. H. Wang, W. Choi and M. S. Strano, *Acs Nano*, 2013, **7**, 6533-6544.
16 H. Hwang, T. Yeo, J. E. Um, K. Y. Lee, H. S. Kim, J. H. Han, W. J. Kim and W. Choi, *Nanoscale Res Lett*, 2014, **9**.
17 T. Yeo, H. Hwang, D. C. Jeong, K. Y. Lee, J. Hong, C. Song and W. Choi, *Nanotechnology*, 2014, **25**.
18 K. Y. Lee, H. Hwang and W. Choi, *Acs Appl Mater Inter*, 2014, **6**, 15575-15582.
19 S. Walia, R. Weber, S. Balendhran, D. Yao, J. T. Abrahamson, S. Zhuiykov, M. Bhaskaran, S. Sriram, M. S. Strano and K. Kalantar-zadeh, *Chem Commun*, 2012, **48**, 7462-7464.
20 S. Walia, S. Balendhran, P. Yi, D. Yao, S. Zhuiykov, M. Pannirselvam, R. Weber, M. S. Strano, M. Bhaskaran, S. Sriram and K. Kalantar-zadeh, *J Phys Chem C*, 2013, **117**, 9137-9142.
21 K. Y. Lee, H. Hwang, D. Shin and W. Choi, *J Mater Chem A*, 2015, **3**, 5457-5466.
22 V. Weiser and N. Eisenreich, *Propell Explos Pyrot*, 2005, **30**, 67-78.
23 Y. P. Sun, K. F. Fu, Y. Lin and W. J. Huang, *Accounts Chem Res*, 2002, **35**, 1096-1104.
24 M. Holzinger, J. Abraha, P. Whelan, R. Graupner, L. Ley, F. Hennrich, M. Kappes and A. Hirsch, *J Am Chem Soc*, 2003, **125**, 8566-8580.
25 Z. H. Yu and L. Brus, *J Phys Chem B*, 2001, **105**, 1123-1134.
26 A. D. Rud, A. M. Lakhnik, S. S. Mikhailova, O. V. Karban, D. V. Surnin and F. Z. Gilmutdinov, *J Alloy Compd*, 2011, **509**, S592-S594.
27 H. B. Yao, Y. Li and A. T. S. Wee, *Appl Surf Sci*, 2000, **158**, 112-119.
28 E. Grigorova, M. Khristov, P. Peshev, D. Nihtianova, N. Veliehkova and G. Atanasova, *Bulg Chem Commun*, 2013, **45**, 280-287.
29 E. J. Setijadi, C. Boyer and K. F. Aguey-Zinsou, *Phys Chem Chem Phys*, 2012, **14**, 11386-11397.
30 M. A. Salam, S. Sufian and T. Murugesan, *Chem Eng Res Des*, 2013, **91**, 2639-2647.
31 K. Y. Lee, M. Kim, Y. W. Lee, J. J. Lee and S. W. Han, *Chem Phys Lett*, 2007, **440**, 249-252.
32 M. Nifuku, S. Koyanaka, H. Ohya, C. Barre, M. Hatori, S. Fujiwara, S. Horiguchi and I. Sochet, *J Loss Prevent Proc*, 2007, **20**, 322-329.
33 M. E. Galvez, A. Frei, G. Albisetti, G. Lunardi and A. Steinfeld, *Int J Hydrogen Energ*, 2008, **33**, 2880-2890.
34 H. R. Byon and H. C. Choi, *Nat Nanotechnol*, 2007, **2**, 162-166.
35 M. Mittal, *J Loss Prevent Proc*, 2014, **27**, 55-64.
36 W. Choi, J. T. Abrahamson, J. M. Strano and M. S. Strano, *Mater Today*, 2010, **13**, 22-33.
37 W. H. Chen, C. Y. Liao and C. I. Hung, *Appl Energ*, 2012, **89**, 464-473.